

ANALYSIS OF RADIATION CHARACTERISTICS OF A PROBE-EXCITED RECTANGULAR RING ANTENNA BY THE DYADIC GREEN'S FUNCTION APPROACH

**S. Lamultree, C. Phongcharoenpanich, S. Kosulvit
and M. Krairiksh**

Faculty of Engineering
King Mongkut's Institute of Technology Ladkrabang
Bangkok 10520, Thailand

Abstract—Radiation characteristics of a probe-excited rectangular ring antenna are investigated by using the dyadic Green's function approach. The radiation characteristics, such as radiation pattern, beam-peak direction, half-power beamwidth and directivity, are analyzed. For the specified operating frequency, the ring width and ring height are selected as the same cross-sectional dimension of rectangular waveguide operated at the dominant mode. The effects of the excited probe and rectangular ring to the modal distributions are described. For the desired modal distribution, the directivity primarily depends on the ring lengths. For compact size of the proposed antenna, the ring length of 0.4λ is chosen to provide a bidirectional pattern with the calculated half-power beamwidth in E -plane and H -plane of 100 and 69 degrees respectively, and directivity of 4.43 dBi. Furthermore, the prototype antenna was fabricated and measured. The coincided results between the theory and the experiment are obtained.

1. INTRODUCTION

Recently, the wireless communications become essential in human activity [1–5]. Therefore, the demand for using a mobile telephone in anywhere is necessary. Generally, the base station antennas in microcellular system for the urban areas are located lower than the surrounded buildings along the streets and located in the underground areas. So, the communicable cell is formed along the street. Therefore, for a base station antenna, a bidirectional antenna is more suitable for the street cell than a typical omnidirectional antenna. Thus, many researches and developments on bidirectional antenna have

been extensively conducted as reviewed in literature [6–11]. From the aforementioned researches, it is evident that development of a bidirectional antenna that has suitable characteristics for a particular application is desired. Moreover, the low cost must be considered since the number of cell is very large. The bidirectional antennas using a linear probe excited circular ring was proposed [12–14] to serve these demands. Although the circular ring provides the slightly higher gain than the rectangular ring, its beamwidth cannot be easily adjusted due to the symmetrical structure. The rectangular ring antenna is very attractive to adjust the beamwidth following the applications by changing the ring width and ring height. Furthermore, the desired directivity is easily obtained by varying the ring length. This paper presents the radiation characteristic investigations of a bidirectional antenna using a probe-excited rectangular ring. The analysis includes the equivalent electric and magnetic current densities. In addition, the position of an excited probe that involves the modal distribution is comprised. Theoretically, there are many techniques to analyze the radiation from the aperture fed by probe in open literature [15–23]. Each method possesses its advantages and disadvantages. In this paper, the dyadic Green's function approach [22–30] is used to analyze the radiation characteristics of the proposed antenna since it is straightforward, and the closed form with physical insight is obtained. The rigorous analysis is expressed in detail.

This paper is organized as follows. Section 2 presents the theory of the antenna including the antenna structure and the derivation expressions. In Section 3, the normalized magnitude of the equivalent electric and magnetic current densities for various modal distributions are shown. The radiation characteristics as the function of antenna parameters are studied. Then, the antenna fabrication and measurement are performed. The experimental results are illustrated in Section 4. Finally, the conclusions are presented in Section 5.

2. THEORY

The proposed antenna consists of a linear electric probe of length l aligned along y direction at the position ($x = s$, $y = -b/2$, $z = 0$). The probe is surrounded by rectangular ring of width a , height b and length c , respectively. There are two apertures at the planes $z = +c/2$ and $z = -c/2$ respectively, as shown in Fig. 1.

The rectangular ring is considered as a part of rectangular waveguide that is truncated at $z = +c/2$ and $z = -c/2$, where the reflection at the aperture of the waveguide ends is omitted. In this paper, the propagation direction and the piloting vector in z

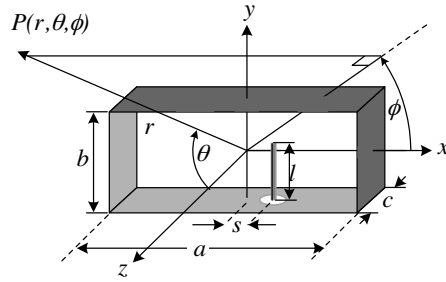


Figure 1. Antenna structure.

direction is assumed. In addition, the time convention $e^{-j\omega t}$ is used and suppressed, where $\omega = 2\pi f$ and f is the frequency. The scalar wave function solved by the method of separation of variables is [24]

$$\psi_{e_{omn}}^{\pm z}(k_z) = \begin{Bmatrix} C_x & C_y \\ S_x & S_y \end{Bmatrix} e^{\mp jk_z z}, \quad \begin{matrix} m = 1, 2, 3, \dots \\ n = 0, 1, 2, \dots \end{matrix} \quad (1)$$

where

$$\begin{aligned} S_x &= \sin\left(k_x\left(x + \frac{a}{2}\right)\right), & C_x &= \cos\left(k_x\left(x + \frac{a}{2}\right)\right), \\ S_y &= \sin\left(k_y\left(y + \frac{b}{2}\right)\right), & C_y &= \cos\left(k_y\left(y + \frac{b}{2}\right)\right), \\ k_x &= \frac{m\pi}{a}, & k_y &= \frac{n\pi}{b}, & k_c &= k_x^2 + k_y^2, & k_z &= \sqrt{k^2 - (k_x^2 + k_y^2)}, \\ k &= \omega\sqrt{\mu_0\epsilon_0}, & \mu_0 &= 4\pi \times 10^{-7} \text{ H/m}, & \epsilon_0 &= 8.854 \times 10^{-12} \text{ F/m}. \end{aligned}$$

The superscript $\pm z$ denotes the field radiations in $+z$ and $-z$ directions, respectively. The subscript e and o are an abbreviation for the even and odd functions, respectively.

The vector wave functions, \overline{M}_{emn} and \overline{N}_{omn} , satisfy the vector Dirichlet boundary condition at the conducting wall ($\overline{a}_n \times \overline{M}_{emn} = 0$ and $\overline{a}_n \times \overline{N}_{omn} = 0$), where \overline{a}_n is the normal unit vector. The vector wave functions \overline{M}_{emn} and \overline{N}_{omn} represent the electric field of TE_{emn} and TM_{omn} modes, respectively. In the same manner, \overline{M}_{omn} and \overline{N}_{emn} are the vector wave functions that satisfy the vector Neumann boundary condition $\overline{a}_n \times \begin{Bmatrix} \nabla \times \overline{M}_{omn} \\ \nabla \times \overline{N}_{emn} \end{Bmatrix} = 0$. Hence, they can be written as

$$\overline{M}_{e_{omn}}(k_z) = \nabla \times \left[\overline{a}_z \psi_{e_{omn}}(k_z) \right] \quad (2)$$

and

$$\bar{N}_{e_{omn}}(k_z) = \frac{1}{k} \nabla \times \nabla \times \left[\bar{a}_z \psi_{e_{omn}}(k_z) \right]. \quad (3)$$

Following the method of magnetic dyadic Green's function and applying the Ohm-Rayleigh method, the magnetic dyadic Green's function due to an electric source ($\bar{\bar{G}}_{HJ}(\bar{R}, \bar{R}')$) that satisfies the dyadic differential equation is

$$\nabla \times \nabla \times \bar{\bar{G}}_{HJ}(\bar{R}, \bar{R}') - k^2 \bar{\bar{G}}_{HJ}(\bar{R}, \bar{R}') = \nabla \times \left[\bar{I} \delta(\bar{R} - \bar{R}') \right]. \quad (4)$$

$\delta(\bar{R} - \bar{R}')$ denotes the Dirac delta function, which is equal to $\delta(x - x') \delta(y - y') \delta(z - z')$ in the Cartesian coordinate. \bar{I} is the unit dyadic. The primed variables (x', y', z') and unprimed variables (x, y, z) are the source point and the observation point, respectively. The relationship in (4) is defined in the domain $-\frac{a}{2} \leq x \leq \frac{a}{2}$, $-\frac{b}{2} \leq y \leq \frac{b}{2}$, $-\infty \leq z \leq \infty$, and the Neumann boundary condition

$$\bar{a}_n \times \nabla \times \bar{\bar{G}}_{HJ}(\bar{R}, \bar{R}') = 0, \quad (5)$$

at $x = -a/2$ and $a/2$, $y = -b/2$ and $b/2$. The eigenfunction expansion of $\bar{\bar{G}}_{HJ}$ in term of the rectangular vector wave functions is given by [24]

$$\begin{aligned} \bar{\bar{G}}_{HJ}(\bar{R}, \bar{R}') = & \int_{-\infty}^{\infty} dk_z \frac{jk}{ab} \sum_{m,n} \frac{(2 - \delta_0) \kappa}{\pi ab k_c^2 (\kappa^2 - k^2)} \left[\bar{N}_{emn}(k_z) \bar{M}'_{emn}(-k_z) \right. \\ & \left. + \bar{M}_{omn}(k_z) \bar{N}'_{omn}(-k_z) \right] \end{aligned} \quad (6)$$

where, $\kappa^2 = \left(\frac{m\pi}{a}\right)^2 + \left(\frac{n\pi}{b}\right)^2 + k_z^2 = k_c^2 + k_z^2$, δ_0 denotes the Kronecker delta function defined as

$$\delta_0 = \begin{cases} 1 & m \text{ or } n = 0 \\ 0 & m \text{ and } n \neq 0 \end{cases} \quad (7)$$

By applying the contour integration, (6) becomes

$$\bar{\bar{G}}_{HJ}^{\pm z}(\bar{R}, \bar{R}') = \begin{cases} -\frac{jk}{ab} \sum_{m,n} \frac{2 - \delta_0}{k_c^2 k_z} \left[\bar{N}_{emn}(+k_z) \bar{M}'_{emn}(-k_z) \right. \\ \quad \left. + \bar{M}_{omn}(+k_z) \bar{N}'_{omn}(-k_z) \right]; & z > z' \\ +\frac{jk}{ab} \sum_{m,n} \frac{2 - \delta_0}{k_c^2 k_z} \left[\bar{N}_{emn}(-k_z) \bar{M}'_{emn}(+k_z) \right. \\ \quad \left. + \bar{M}_{omn}(-k_z) \bar{N}'_{omn}(+k_z) \right]; & z < z'. \end{cases} \quad (8)$$

The electric dyadic Green's function due to an electric source $\overline{\overline{G}}_{EJ}(\overline{R}, \overline{R}')$ is obtained from the relationship

$$\nabla \times \overline{\overline{G}}_{HJ}(\overline{R}, \overline{R}') = \overline{\overline{I}}\delta(\overline{R} - \overline{R}') + k^2 \overline{\overline{G}}_{EJ}(\overline{R}, \overline{R}'). \quad (9)$$

Then, we obtain

$$\begin{aligned} \overline{\overline{G}}_{EJ}^{\pm z}(\overline{R}, \overline{R}') &= -\overline{a}_z \overline{a}_z \frac{1}{k^2} \delta(\overline{R} - \overline{R}') \\ &+ \begin{cases} -\frac{j}{ab} \sum_{m=1}^{\infty} \sum_{n=0}^{\infty} \frac{2 - \delta_0}{k_c^2 k_z} [\overline{M}_{emn}(+k_z) \overline{M}'_{emn}(-k_z) \\ + \overline{N}_{omn}(+k_z) \overline{N}'_{omn}(-k_z)]; & z > z' \\ +\frac{j}{ab} \sum_{m=1}^{\infty} \sum_{n=0}^{\infty} \frac{2 - \delta_0}{k_c^2 k_z} [\overline{M}_{emn}(-k_z) \overline{M}'_{emn}(+k_z) \\ + \overline{N}_{omn}(-k_z) \overline{N}'_{omn}(+k_z)]; & z < z', \end{cases} \quad (10) \end{aligned}$$

$$\overline{M}_{emn}^{\pm z}(k_z) = (-\overline{a}_x k_y C_x S_y + \overline{a}_y k_x S_x C_y) e^{\mp j k_z z}, \quad (11)$$

$$\begin{aligned} \overline{N}_{omn}^{\pm z}(k_z) &= \frac{1}{\kappa} (\mp \overline{a}_x j k_z k_x C_x S_y \mp \overline{a}_y j k_z k_y S_x C_y \\ &+ \overline{a}_z k_c^2 S_x S_y) e^{\mp j k_z z}, \quad (12) \end{aligned}$$

$$\overline{M}_{omn}^{\pm z}(k_z) = (\overline{a}_x k_y S_x C_y - \overline{a}_y k_x C_x S_y) e^{\mp j k_z z} \quad (13)$$

and

$$\overline{N}_{emn}^{\pm z}(k_z) = \frac{1}{\kappa} (\pm \overline{a}_x j k_z k_x S_x C_y \pm \overline{a}_y j k_z k_y C_x S_y + \overline{a}_z k_c^2 C_x C_y) e^{\mp j k_z z}. \quad (14)$$

The electric field ($\overline{E}(\overline{R})$) inside the ring with the probe excitation is determined by using

$$\overline{E}^{\pm z}(\overline{R}) = \mp j \omega \mu_0 \iiint_V \overline{\overline{G}}_{EJ}^{\pm}(\overline{R}, \overline{R}') \cdot \overline{J}(\overline{R}') dV', \quad (15)$$

where $\overline{\overline{G}}_{EJ}^{\pm}(\overline{R}, \overline{R}')$ is obtained from (10) and $\overline{J}(\overline{R}')$ is the electric current distribution along the probe. In this paper, the linear probe directed in y direction has a small diameter compared to the wavelength and the sinusoidal distribution is reasonably assumed as

$$\overline{J}(\overline{R}') = \overline{a}_y \frac{I_m}{d} \sin k \left(l - y' - \frac{b}{2} \right), \quad (16)$$

where I_m is the maximum current that is normalized to be unity and d is the diameter of the probe. Since the probe is oriented in y direction, hence only G_{EJ}^{xy} , G_{EJ}^{yy} , and G_{EJ}^{zy} can contribute to the electric field. All of these components are derived and shown as

$$G_{EJ}^{xy, \pm z} = \begin{cases} -\frac{j}{ab} \sum_{m=1}^{\infty} \sum_{n=0}^{\infty} \frac{2 - \delta_0}{k_c^2 k_z} (-k_x k_y C_x S_y S'_x C'_y \\ + \frac{1}{\kappa^2} k_z^2 k_x k_y C_x S_y S'_x C'_y) e^{-jk_z(z-z')}; & z > z' \\ \frac{j}{ab} \sum_{m=1}^{\infty} \sum_{n=0}^{\infty} \frac{2 - \delta_0}{k_c^2 k_z} (-k_x k_y C_x S_y S'_x C'_y \\ + \frac{1}{\kappa^2} k_z^2 k_x k_y C_x S_y S'_x C'_y) e^{+jk_z(z'-z)}; & z < z', \end{cases} \quad (17)$$

$$G_{EJ}^{yy, \pm z} = \begin{cases} -\frac{j}{ab} \sum_{m=1}^{\infty} \sum_{n=0}^{\infty} \frac{2 - \delta_0}{k_c^2 k_z} (k_x^2 S_x C_y S'_x C'_y \\ + \frac{1}{\kappa^2} k_z^2 k_y^2 S_x C_y S'_x C'_y) e^{-jk_z(z-z')}; & z > z' \\ \frac{j}{ab} \sum_{m=1}^{\infty} \sum_{n=0}^{\infty} \frac{2 - \delta_0}{k_c^2 k_z} (k_x^2 S_x C_y S'_x C'_y \\ + \frac{1}{\kappa^2} k_z^2 k_y^2 S_x C_y S'_x C'_y) e^{+jk_z(z'-z)}; & z < z' \end{cases} \quad (18)$$

and

$$G_{EJ}^{zy, \pm z} = \begin{cases} -\frac{j}{ab} \sum_{m=1}^{\infty} \sum_{n=0}^{\infty} \frac{2 - \delta_0}{k_c^2 k_z} \frac{j}{\kappa^2} k_c^2 k_z k_y S_x S_y S'_x C'_y e^{-jk_z(z-z')}; & z > z' \\ \frac{j}{ab} \sum_{m=1}^{\infty} \sum_{n=0}^{\infty} \frac{2 - \delta_0}{k_c^2 k_z} \left(-\frac{j}{\kappa^2}\right) k_c^2 k_z k_y S_x S_y S'_x C'_y e^{+jk_z(z'-z)}; & z < z'. \end{cases} \quad (19)$$

Consequently, the electric field in x , y , and z components are

$$E_x^{\pm z} = -\frac{\omega \mu_0 I_m}{abd} \sum_{m=1}^{\infty} \sum_{n=0}^{\infty} \left\{ \frac{2 - \delta_0}{k_c^2 k_z} (-k) \sin \left(k_x \left(s + \frac{a}{2} \right) \right) \right. \\ \times \left(\frac{\cos(k_y l) - \cos(kl)}{k_y^2 - k^2} \right) \left(-k_x k_y + \frac{k_z^2 k_x k_y}{\kappa^2} \right) \\ \left. \times \cos \left(k_x \left(x + \frac{a}{2} \right) \right) \sin \left(k_y \left(y + \frac{b}{2} \right) \right) e^{-jk_z z} \right\}, \quad (20)$$

$$\begin{aligned}
E_y^{\pm z} &= -\frac{\omega\mu_0 I_m}{abd} \sum_{m=1}^{\infty} \sum_{n=0}^{\infty} \left\{ \frac{2-\delta_0}{k_c^2 k_z} (-k) \sin\left(k_x \left(s + \frac{a}{2}\right)\right) \right. \\
&\quad \times \left(\frac{\cos(k_y l) - \cos(kl)}{k_y^2 - k^2} \right) \left(k_x^2 + \frac{k_z^2 k_y^2}{\kappa^2} \right) \\
&\quad \left. \times \sin\left(k_x \left(x + \frac{a}{2}\right)\right) \cos\left(k_y \left(y + \frac{b}{2}\right)\right) e^{-jk_z z} \right\} \quad (21)
\end{aligned}$$

and

$$\begin{aligned}
E_z^{\pm z} &= -j \frac{\omega\mu_0 I_m}{abd} \sum_{m=1}^{\infty} \sum_{n=0}^{\infty} \left\{ \frac{2-\delta_0}{\kappa^2} (-k) \sin\left(k_x \left(s + \frac{a}{2}\right)\right) \right. \\
&\quad \times \left(\frac{\cos(k_y l) - \cos(kl)}{k_y^2 - k^2} \right) k_y \sin\left(k_x \left(x + \frac{a}{2}\right)\right) \\
&\quad \left. \times \sin\left(k_y \left(y + \frac{b}{2}\right)\right) e^{-jk_z z} \right\}. \quad (22)
\end{aligned}$$

The equivalent magnetic current densities (\overline{M}_s) at the two apertures are obtained from

$$\overline{M}_s^{\pm z}(\overline{R}) = \overline{E}^{\pm z}(\overline{R}) \Big|_{z=\pm c/2} \times (\pm \overline{a}_z) \quad (23)$$

The resultant equivalent magnetic current densities are

$$\begin{aligned}
\overline{M}_s^{\pm z}(\overline{R}) &= -\frac{\omega\mu_0 I_m}{abd} \sum_{m=1}^{\infty} \sum_{n=0}^{\infty} \left\{ \frac{2-\delta_0}{k_c^2 k_z} (-k) \sin\left(k_x \left(s + \frac{a}{2}\right)\right) \right. \\
&\quad \times \left(\frac{\cos(k_y l) - \cos(kl)}{k_y^2 - k^2} \right) e^{-jk_z z} \left\{ \pm \overline{a}_x \left[\left(k_x^2 + \frac{k_z^2 k_y^2}{\kappa^2} \right) \right. \right. \\
&\quad \times \sin\left(k_x \left(x + \frac{a}{2}\right)\right) \cos\left(k_y \left(y + \frac{b}{2}\right)\right) \left. \right] \mp \overline{a}_y \left[\left(-k_x k_y + \frac{k_z^2 k_x k_y}{\kappa^2} \right) \right. \\
&\quad \left. \left. \times \cos\left(k_x \left(x + \frac{a}{2}\right)\right) \sin\left(k_y \left(y + \frac{b}{2}\right)\right) \right] \right\} \right\}. \quad (24)
\end{aligned}$$

By following the same fashion, the magnetic field ($\overline{H}(\overline{R})$) can be found from

$$\overline{H}(\overline{R}) = \iiint_V \overline{\overline{G}}_{HJ}(\overline{R}, \overline{R}') \cdot \overline{J}(\overline{R}') dV' \quad (25)$$

where $\overline{\overline{G}}_{HJ}$, after some mathematical manipulations, can be derived as

$$G_{HJ}^{xy, \pm z} = \frac{k}{ab} \sum_{m=1}^{\infty} \sum_{n=0}^{\infty} \frac{(2 - \delta_0)}{k_c^2 \kappa} S_x C_y S'_x C' \times \begin{cases} (k_x^2 + k_y^2) e^{-jk_z(z-z')}; & z > z' \\ (-k_x^2 - k_y^2) e^{+jk_z(z'-z)}; & z < z', \end{cases} \quad (26)$$

$$G_{HJ}^{yy, \pm z} = 0 \quad (27)$$

and

$$G_{HJ}^{zy, \pm z} = \begin{cases} -\frac{jk}{ab} \sum_{m=1}^{\infty} \sum_{n=0}^{\infty} \frac{(2 - \delta_0)}{k_c^2 k_z \kappa} k_c^2 k_x C_x S_y S'_x S'_y e^{-jk_z(z-z')}; & z > z' \\ \frac{jk}{ab} \sum_{m=1}^{\infty} \sum_{n=0}^{\infty} \frac{(2 - \delta_0)}{k_c^2 k_z \kappa} k_c^2 k_x C_x S_y S'_x S'_y e^{+jk_z(z'-z)}; & z < z'. \end{cases} \quad (28)$$

The magnetic field components are

$$H_x^{\pm z} = \pm \frac{kI_m}{abd} \sum_{m=1}^{\infty} \sum_{n=0}^{\infty} \left\{ \frac{(2 - \delta_0)}{\kappa k_c^2} (-k) \sin \left(k_x \left(s + \frac{a}{2} \right) \right) \times \left(\frac{\cos(k_y l) - \cos(kl)}{(k_y^2 - k^2)} \right) e^{-jk_z z} (k_x^2 + k_y^2) \times \sin \left(k_x \left(x + \frac{a}{2} \right) \right) \cos \left(k_y \left(y + \frac{b}{2} \right) \right) \right\}, \quad (29)$$

$$H_y^{\pm z} = 0 \quad (30)$$

and

$$H_z^{\pm z} = \mp j \frac{kI_m}{abd} \sum_{m=1}^{\infty} \sum_{n=0}^{\infty} \left\{ \frac{(2 - \delta_0)}{\kappa k_c^2} (-k) \sin \left(k_x \left(s + \frac{a}{2} \right) \right) \times \left(\frac{\cos(k_y l) - \cos(kl)}{(k_y^2 - k^2)} \right) e^{-jk_z z} \times \frac{k_x k_c^2}{k_z} \cos \left(k_x \left(x + \frac{a}{2} \right) \right) \cos \left(k_y \left(y + \frac{b}{2} \right) \right) \right\}. \quad (31)$$

Similarly, the equivalent electric current densities ($\overline{\overline{J}}_s$) are

$$\overline{\overline{J}}_s^{\pm z} (\overline{\overline{R}}) = \pm \overline{\overline{a}}_z \times \overline{\overline{H}} (\overline{\overline{R}}) \Big|_{z=\pm c/2} \quad (32)$$

and

$$\begin{aligned} \overline{J}_s^{\pm z}(\overline{R}) = & \frac{kI_m}{abd} \sum_{m=1}^{\infty} \sum_{n=0}^{\infty} \left\{ \frac{2 - \delta_0}{k_c^2 \kappa} (-k) \sin \left(k_x \left(s + \frac{a}{2} \right) \right) \right. \\ & \times \left(\frac{\cos(k_y l) - \cos(kl)}{k_y^2 - k^2} \right) (k_x^2 + k_y^2) e^{-jk_z z} \\ & \left. \times \left[\pm \overline{a}_y \sin \left(k_x \left(x + \frac{a}{2} \right) \right) \cos \left(k_y \left(y + \frac{b}{2} \right) \right) \right] \right\}. \quad (33) \end{aligned}$$

After the equivalent magnetic and electric current densities are readily obtained, the far-zone radiated field from a probe-excited rectangular ring antenna can be subsequently found by using radiation parameters from [31]. By neglecting mutual coupling and reflection at the edge of the ring and assuming that there is no reflection from the opposite aperture, a superposition of the fields from the two apertures can be applied. The fields radiated from the two apertures are combined with the same phase but in opposite directions. The resultant field can be written as follows

$$E_{\theta}^{\pm z}(r, \theta, \phi) \simeq -\frac{jk e^{-jk(r \mp \frac{c}{2} \cos \theta)}}{4\pi r} \left(L_{\phi}^{\pm z} + \eta N_{\theta}^{\pm z} \right), \quad (34)$$

$$E_{\phi}^{\pm z}(r, \theta, \phi) \simeq +\frac{jk e^{-jk(r \mp \frac{c}{2} \cos \theta)}}{4\pi r} \left(L_{\theta}^{\pm z} - \eta N_{\phi}^{\pm z} \right) \quad (35)$$

and

$$\begin{aligned} |E_{Total}(r, \theta, \phi)| = & \left\{ \left(E_{\theta}^{+z}(r, \theta, \phi) + E_{\theta}^{-z}(r, \theta, \phi) \right)^2 \right. \\ & \left. + \left(E_{\phi}^{+z}(r, \theta, \phi) + E_{\phi}^{-z}(r, \theta, \phi) \right)^2 \right\}^{1/2}, \quad (36) \end{aligned}$$

where

$$\begin{aligned} N_{\theta}^{\pm z} = & \pm \frac{kI_m}{abd} \sum_{m=1}^{\infty} \sum_{n=0}^{\infty} \left\{ \frac{2 - \delta_0}{k_c^2 \kappa} \frac{ab}{4j} (-k) \sin \left(k_x \left(s + \frac{a}{2} \right) \right) \right. \\ & \times \left(\frac{\cos(k_y l) - \cos(kl)}{k_y^2 - k^2} \right) e^{-jk_z z'} \left[\pm (k_x^2 + k_y^2) \cos \theta \sin \phi \right. \\ & \left. \left. \times (SA - SA') (SB + SB') \right] \right\}, \quad (37) \end{aligned}$$

$$\begin{aligned}
N_{\phi}^{\pm z} &= \pm \frac{k I_m}{abd} \sum_{m=1}^{\infty} \sum_{n=0}^{\infty} \left\{ \frac{2 - \delta_0}{k_c^2 \kappa} \frac{ab}{4j} (-k) \sin \left(k_x \left(s + \frac{a}{2} \right) \right) \right. \\
&\quad \times \left(\frac{\cos(k_y l) - \cos(kl)}{k_y^2 - k^2} \right) e^{-jk_z z'} [\pm (k_x^2 + k_y^2) \cos \phi \\
&\quad \times (SA - SA') (SB + SB')] \left. \right\}, \tag{38}
\end{aligned}$$

$$\begin{aligned}
L_{\theta}^{\pm z} &= -\frac{\omega \mu_0 I_m}{abd} \sum_{m=1}^{\infty} \sum_{n=0}^{\infty} \left\{ \frac{2 - \delta_0}{k_c^2 k_g} \frac{ab}{4j} (-k) \sin \left(k_x \left(s + \frac{a}{2} \right) \right) \right. \\
&\quad \times \left(\frac{\cos(k_y l) - \cos(kl)}{k_y^2 - k^2} \right) e^{-jk_z z'} \left[\pm \left(k_x^2 + \frac{k_z^2 k_y^2}{\kappa^2} \right) \cos \theta \cos \phi \right. \\
&\quad \times (SA - SA') (SB + SB') \mp \left(-k_x k_y + \frac{k_z^2 k_x k_y}{\kappa^2} \right) \\
&\quad \left. \left. \times \cos \theta \sin \phi (SA + SA') (SB - SB') \right] \right\} \tag{39}
\end{aligned}$$

and

$$\begin{aligned}
L_{\phi}^{\pm z} &= -\frac{\omega \mu_0 I_m}{abd} \sum_{m=1}^{\infty} \sum_{n=0}^{\infty} \left\{ \frac{2 - \delta_0}{k_c^2 k_g} \frac{ab}{4j} (-k) \right. \\
&\quad \times \sin \left(k_x \left(s + \frac{a}{2} \right) \right) \left(\frac{\cos(k_y l) - \cos(kl)}{k_y^2 - k^2} \right) e^{-jk_z z'} \\
&\quad \times \left[\mp \left(k_x^2 + \frac{k_z^2 k_y^2}{\kappa^2} \right) \sin \phi (SA - SA') (SB + SB') \right. \\
&\quad \left. \mp \left(-k_x k_y + \frac{k_z^2 k_x k_y}{\kappa^2} \right) \cos \phi (SA + SA') (SB - SB') \right] \left. \right\}. \tag{40}
\end{aligned}$$

where

$$\begin{aligned}
SA &= \frac{\sin [(a/2) (k \sin \theta \cos \phi + k_x)]}{a/2 (k \sin \theta \cos \phi + k_x)} e^{jk_x a/2}, \\
SA' &= \frac{\sin [(a/2) (k \sin \theta \cos \phi - k_x)]}{a/2 (k \sin \theta \cos \phi - k_x)} e^{-jk_x a/2}, \\
SB &= \frac{\sin [(b/2) (k \sin \theta \sin \phi + k_y)]}{b/2 (k \sin \theta \sin \phi + k_y)} e^{jk_y b/2} \\
\text{and } SB' &= \frac{\sin [(b/2) (k \sin \theta \sin \phi - k_y)]}{b/2 (k \sin \theta \sin \phi - k_y)} e^{-jk_y b/2}.
\end{aligned}$$

Consequently, the far-field radiation of the antenna can be expressed by substituting (37)–(40) into (34)–(35).

3. RADIATION CHARACTERISTICS

The total electric field is obtained from the summation of electric field distribution of a probe excited rectangular ring antenna as written in (20)–(22), (29)–(31) and (36). It should be pointed that considering the minimum number of summation terms of m and n , that provide efficiently accurate results for minimizing the running time of the computed results, is important. Therefore, the appropriate number of m and n for the numerical convergence should be obtained. Fig. 2 shows the number of summation m and n for various c . The criterion of convergence consideration is that the deviation of half-power beamwidth of the antenna is less than 0.5 degree. Apparently, the number of summation m and n should be larger ($m = 7$ and $n = 1$) for the shorter c , due to the influence of the higher order modes. The number of summation m and n will be decreased to 1 and 0 respectively, for the larger c because the higher order modes are reduced rapidly. For the dominant mode ($m = 1$ and $n = 0$) the magnitude of current densities keeps almost constant (see Fig. 3). Thus, it is obvious that $m = 7$ and $n = 1$ will be used for all ring lengths. These values are used to obtain the characteristics of the antenna that are explicitly expressed hereafter. From the total fields of the antenna as shown in (36), it is obvious that the radiation characteristics of the antenna depend on the following parameters, i.e., probe position (s), probe length (l), ring width (a), ring height (b) and ring length (c). In this paper, the initial probe length is 0.25λ for the reason of good impedance matching. Since the cross-section of the antenna is the same as a rectangular waveguide, in this circumstance the ring width and ring height are chosen to be the dimension of a standard waveguide operating at the dominant mode.

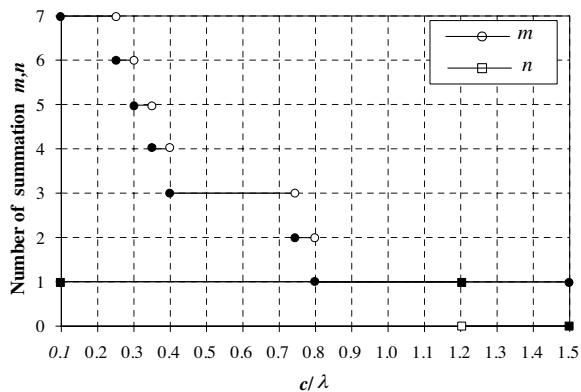


Figure 2. The number of summation m and n for various ring lengths.

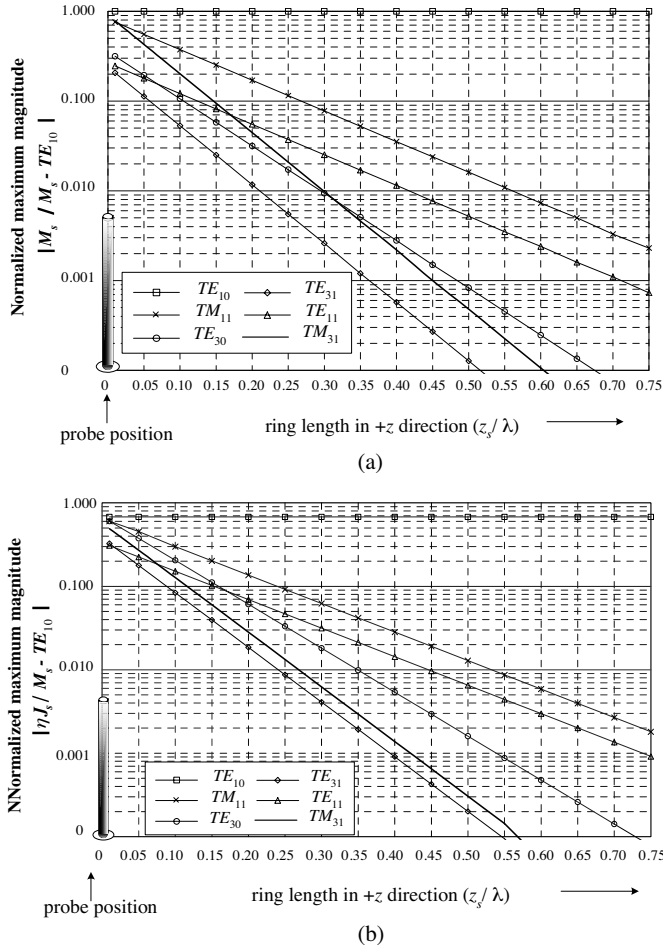


Figure 3. Normalized magnitude of M_s and ηJ_s for various aperture distances z_s (where probe is located at $(x = s = 0, y = -b/2, z = 0)$): (a) M_s , (b) ηJ_s .

Thus, the ring width of a , and ring height of $b = a/R$ are selected, where R is the ratio of a/b and $R \geq 1$; in this paper $R = 2$ is used. The cut-off wavelength is obtained from [32]

$$\lambda_c = \frac{2\pi}{\sqrt{\left(\frac{m\pi}{a}\right)^2 + \left(\frac{n\pi}{b}\right)^2}}. \quad (41)$$

Thus, a choice of TE₁₀ mode is restricted in the range of $\frac{\lambda}{2} < a < \lambda$. It is noted that a should be far away from the upper range to avoid higher modes. Thenceforth, $a = 0.70\lambda$ and $b = 0.35\lambda$ are selected, and these values are fixed throughout this paper. Accordingly, the antenna characteristics depend on the ring length.

Following (20)–(22) and (29)–(31), the equivalent current densities of the antenna are determined. It is revealed that a short ring length contains several modes in the vicinity of the probe and the evanescent waves of the higher order modes near the probe still have a considerable level at the aperture as shown in Fig. 3. Furthermore, the TE₁₀ mode keeps the constant value for any z_s (where z_s is the distance of $c/2$ away from the probe position), whereas the higher order modes are lower as the further distance to the aperture. They reduce rapidly when $z_s = 0.75\lambda$. In addition, it is found that some modes do not exist especially the modes with even m , that is different from those in the rectangular waveguide. However, the modes with even m are induced and strengthen when probe is shifted from the center ($x = s = 0$, $y = -b/2$, $z = 0$) whereas modes with odd m are decreased as shown in Fig. 4. The dominant mode TE₁₀ is still stronger than the others. It should be noted that modal distribution inside a probe-excited rectangular ring antenna also has strong effect to the input impedance of the proposed antenna that is left for further study.

According to (34)–(40) in Section 2, the electric fields are plotted. Fig. 5 shows the radiation pattern of the antenna as a function of c . The radiation pattern of a single aperture in $+z$ and $-z$ directions at $z_s = \pm c/2$ is shown for the condition of the field that only radiates toward $+z$ and $-z$ directions and there is no coupling between the apertures. Then, radiation pattern from two apertures is displayed from the combination of a single aperture in $+z$ and $-z$ directions. It should be noted that the dummy load is terminated at the aperture of $-z$ and $+z$ directions for considering radiation pattern radiated from the aperture of $+z$ and $-z$ directions, respectively. The bidirectional pattern can be produced. It is observed that for the c shorter than 0.1λ , the radiated field is same as the pattern of a dipole antenna, viz., the E -plane pattern ($\phi = 90^\circ$) approaches figure of eight and almost omnidirectional pattern in H -plane ($\phi = 0^\circ$). Moreover, by increasing c , the pattern in E -plane is wider and then split. Then it becomes a bidirectional pattern with side lobes. The H -plane pattern has wider beam for the shorter c because the aperture separation affects the radiation patterns. In addition, the E -plane pattern has null and the H -plane pattern broadens at $\theta = 90^\circ$ due to the effect of the ring edge. It can be considered that the omnidirectional pattern of linear monopole (probe) is forced to radiate only in forward and backward

directions to form bidirectional pattern.

In addition, the beam-peak direction of E -plane will be slightly tilted from z axis ($\theta = 0^\circ$ and $\theta = 180^\circ$) due to the influence of asymmetrical probe position at the upper and lower side (i.e., it is located at the lower side) as shown in Fig. 6. It is found that a bidirectional pattern is obtained at $c \leq 0.6\lambda$ and will occur again with existed side lobe at $c \geq 1.25\lambda$ (for the beam peak directs $+5$ and -5 degrees tilted from z axis). Furthermore, in Fig. 6, the half-power beamwidth in the E -plane and the H -plane have the opposite curve, viz., a wider beamwidth and a narrower beamwidth in E -plane and H -

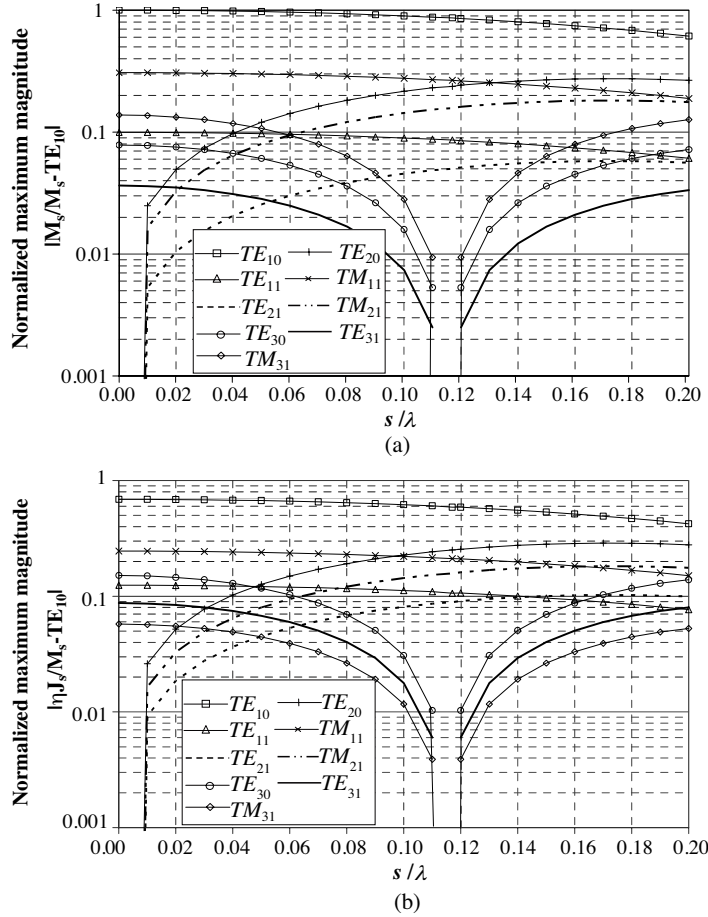


Figure 4. Normalized magnitude of M_s and ηJ_s for various s (where probe is located at $(x = s, y = -b/2, z = 0)$): (a) M_s , (b) ηJ_s .

plane respectively, as the longer ring length except at $c \geq 1.3\lambda$. These result to the directivity of the antenna that will be then described. Note that the narrow beamwidth is required for the high directivity.

The directivity is a figure of merit that quantifies the antenna directive properties comparing with an isotropic antenna. The maximum directivity is defined as the maximum radiation intensity of that antenna (U_{\max}) over the radiation intensity of isotropic radiator ($P_{\text{rad}}/4\pi$). The high radiation intensity with the low radiated power is required to enhance directivity. The maximum radiation intensity is obtained from combining of the maximum amplitude of electric field

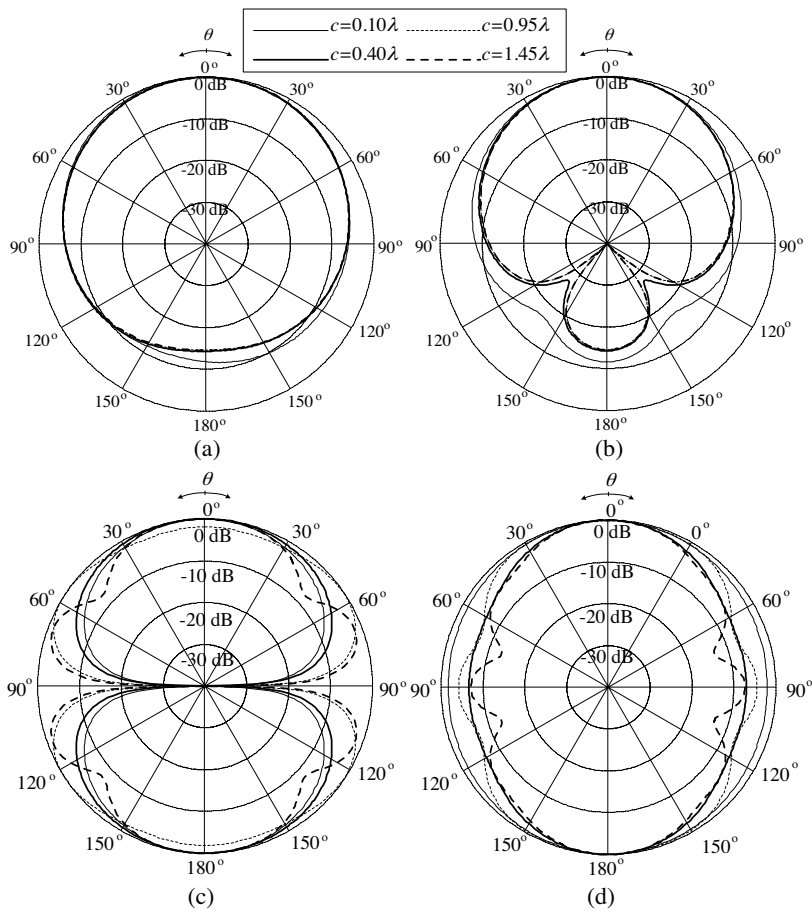


Figure 5. Radiation pattern for various c : (a) E -plane of $+z$ aperture, (b) H -plane of $+z$ aperture, (c) E -plane of two apertures, (d) H -plane of two apertures.

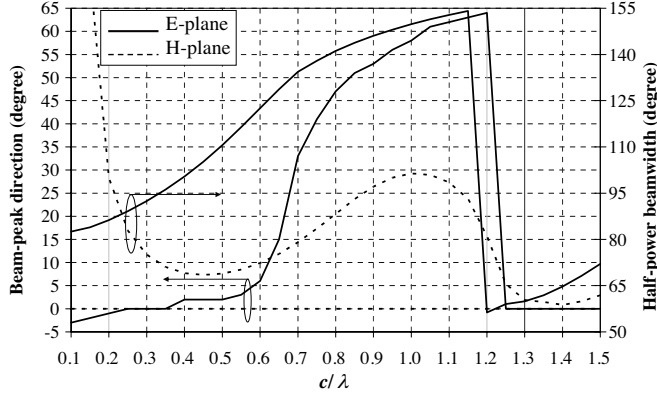


Figure 6. Beam-peak direction and half-power beamwidth for various ring lengths.

that radiates from $+z$ and $-z$ apertures as

$$\begin{aligned}
 |\overline{E}|^2 &= |E_{\theta,+z} + E_{\theta,-z}|^2 + |E_{\phi,+z} + E_{\phi,-z}|^2 \\
 &= \left(|E_{\theta,+z}|^2 + |E_{\theta,-z}|^2 + 2|E_{\theta,+z}||E_{\theta,-z}|\cos(\xi_{\theta,+z} - \xi_{\theta,-z}) \right) \\
 &\quad + \left(|E_{\phi,+z}|^2 + |E_{\phi,-z}|^2 + 2|E_{\phi,+z}||E_{\phi,-z}|\cos(\xi_{\phi,+z} - \xi_{\phi,-z}) \right). \quad (42)
 \end{aligned}$$

The optimum ring length that provides the maximum directivity must be clarified. Fig. 7 shows the maximum directivity as a function of ring length when $l = 0.25\lambda$, $a = 0.70\lambda$ and $b = 0.35\lambda$. In Fig. 7(a), it can be seen that the maximum radiation intensity can be found at $\theta = 0^\circ$ and $\phi = 90^\circ$ by combining the square of magnitude of electric field aperture at $+z$ ($|E_{\theta,+z}|^2$) and $-z$ directions ($|E_{\theta,-z}|^2$) respectively, with the term of phase difference ($\xi_{+z} - \xi_{-z}$) between $+z$ and $-z$ apertures, as defined by subscript $+z$ and $-z$, respectively. Equation (42) shows that E_ϕ has null in this direction. Therefore, only a component of E_θ is shown in Fig. 7(a). The term of phase difference has more impact on radiation intensity. Nevertheless, at the maximum intensity ($c = 0.5\lambda$), the radiated power is rather high. Hence the maximum directivity does not occur as in Fig. 7(b). Furthermore, the mode distributions inside the ring also affect to the directivity; i.e., the shorter c provides the high magnitude of higher order mode, and the directivity is decreased. Furthermore, the aperture separation also influences to the directivity. As the results, the highest directivity of 4.60 dBi for $c = 1.4\lambda$ is achieved because this length provides

the narrower beamwidth with existed side lobe. However, for the bidirectional pattern with no side lobe, the appropriated ring length of 0.4λ provides the directivity of 4.43 dBi. For the compact size of antenna, the ring length of 0.4λ is chosen.

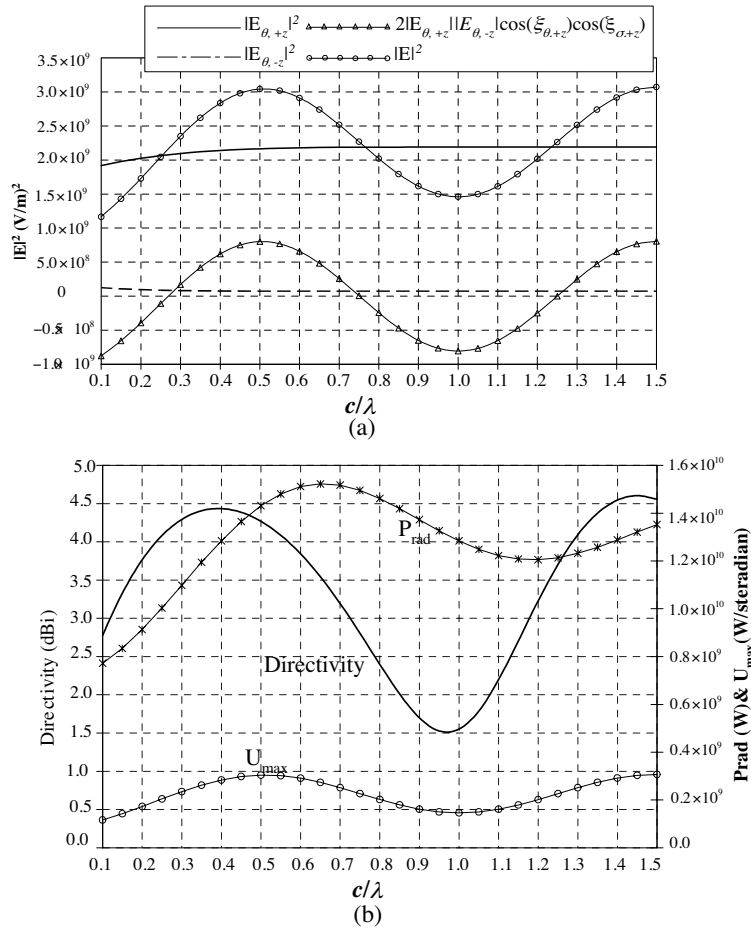


Figure 7. Directivity, radiated power and radiation intensity for various ring lengths: (a) Magnitude of radiated field. (b) Directivity, P_{rad} and U_{max} .

4. EXPERIMENTS

To verify the calculated results by using the dyadic Green's function approach, the numerical results from Method of Moments (MoM) with the Rao-Wilton-Glisson (RWG) basis functions [33] and measured results are compared. It is noted that using RWG-MoM, the mutual coupling and reflection from the edges of ring is taken into account. However, the computation time for RWG-MoM is results, 4.47 times longer than that from the dyadic Green's function approach. One reason is that the closed form is not available for RWG-MoM. For the experiment, a prototype antenna was fabricated with the designed parameters as pointed in the previous section to operate at the operating frequency of 1.9 GHz. The ring was made of brass of 1 mm thickness with the dimension of the ring height equals 5.5 cm and the ring width equals 11.0 cm. The ring length is 6.3 cm. This structure was excited by a linear electric probe made of copper rod with the diameter of 2 mm. The probe length was 4.3 cm and was located at $(x = s = 0.4 \text{ cm}, y = -b/2, z = 0)$ for impedance matching. This probe was connected to a transmission line via an N type connector. The photograph of the fabricated antenna is shown in Fig. 8. The radiation patterns of the antenna were measured by using an HP8720C Network Analyzer.

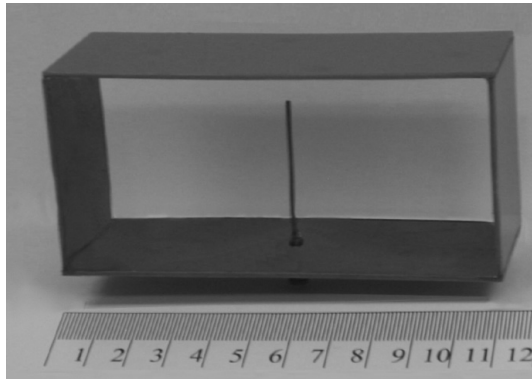


Figure 8. Photograph of the prototype antenna.

Fig. 9(a) and Fig. 9(b) show the calculated and measured radiations in E -plane and H -plane, respectively. It is found that the ofmeasured results in both E -plane and H -plane fairly coincide between the results from dyadic Green's function approach and RWG-MoM. At $\theta = 90^\circ$ region in H -plane, the null from RWG-MoM is deeper than that from the dyadic Green's function approach because

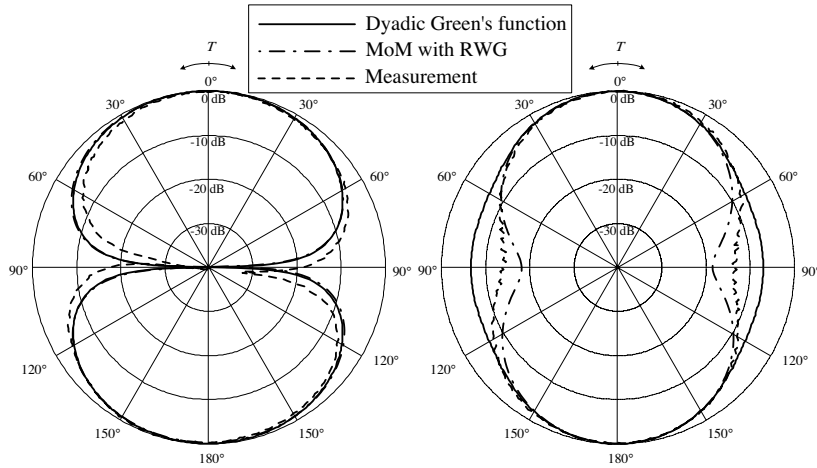


Figure 9. Measured and calculated results of radiation pattern for $c = 0.4\lambda$: (a) E -plane, (b) H -plane.

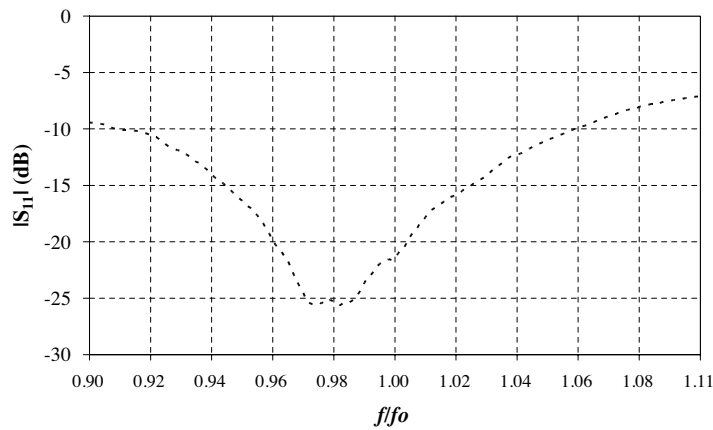


Figure 10. Measured $|S_{11}|$ of the antenna.

the effect of mutual coupling and edge reflection that is neglected from the dyadic Green's function approach. Furthermore, the beam-peak directions in E -plane from dyadic Greens function, RWG-MoM and measurement direct at 1, 1 and 3 degrees, respectively. For H -plane, the beam peak points at the same direction of 0 degree. In addition, the bidirectional pattern is achieved with the computed half-power beamwidth in E -plane of 100 degree and H -plane of 69 degree

from dyadic Green's function approach compared with the measured half-power beamwidth in E -plane and H -plane of 90 and 67 degrees respectively. The simulation from RWG-MoM provides half-power beamwidth in E -plane and H -plane of 106 and 70 degrees, respectively. Furthermore, it is found that at $(\theta = 0^\circ, \phi = 90^\circ)$ the gains of 4.43 dBi, 4.72 dBi and 4.40 dBi are yielded from the dyadic Green's function approach, RWG-MoM and measurement, respectively.

It should be noted that the impedance characteristic is not aimed in this paper; however, the $|S_{11}|$ of the antenna was measured to clarify the matching condition as shown in Fig. 10. It is found that $|S_{11}|$ is -21.5 dB (lower than -10 dB) at the operating frequency. The measured bandwidth ($|S_{11}| < -10$ dB) and gain are 16% and 4.40 dBi, respectively.

5. CONCLUSIONS

This paper presents the investigations of a bidirectional antenna using a probe-excited rectangular ring by using the dyadic Green's function approach. The antenna characteristics depend on the probe length, ring width, ring height and ring length. In addition, the bidirectional patterns without side lobes are obtained for the appropriated ring length c from 0.10λ to 0.65λ . The side lobe is occurred when $c \geq 1.25\lambda$. Furthermore, the beam-peak direction in E -plane is slightly tilted from z -axis because the probe position is not symmetry between the upper and lower sides of the ring. For H -plane pattern, the beam directs in $+z$ and $-z$ directions for any ring length of interest because of the symmetrical geometry in its plane. For the specified cross-sectional dimensions, the ring length is selected to achieve the optimum radiation pattern. Furthermore, the experiment was set up to verify the theoretical predictions. Apparently, the measured radiation pattern coincided with the calculated result except at around $\theta = 90^\circ$ due to the edge effect. The computed directivity of 4.43 dBi and measured gain of 4.40 dBi are obtained. The polarization of this antenna at the directions along the street cell ($+z$ and $-z$ directions) is linear because there is only one component of electric field. Although the sinusoidal current distributions, disregarded mutual coupling and omitted reflection at the edge of the ring is assumed, the experimental results provide the validity of the theoretical predictions.

ACKNOWLEDGMENT

This work was supported by the Thailand Research Fund (TRF) under the grant number RTA5180002.

REFERENCES

1. Huang, C.-W. P., A. Z. Elsherbeni, J. J. Chen, and C. E. Smith, "FDTD characterization of meander line antennas for RF and wireless communications," *Progress In Electromagnetics Research*, PIER 24, 185–199, 1999.
2. Wang, Y. J. and C. K. Lee, "Design of dual-frequency microstrip patch antennas and application for IMT-2000 mobile handsets," *Progress In Electromagnetics Research*, PIER 36, 265–278, 2002.
3. Eldek, A. A., A. Z. Elsherbeni, and C. E. Smith, "Dual-wideband square slot antenna with a U-shaped printed tuning stub for personal wireless communication systems," *Progress In Electromagnetics Research*, PIER 53, 319–333, 2005.
4. Song, Y., Y.-C. Jiao, G. Zhao, and F.-S. Zhang, "Multiband CPW-FED triangle-shaped monopole antenna for wireless applications," *Progress In Electromagnetics Research*, PIER 70, 329–336, 2007.
5. Si, L.-M. and X. Lv, "CPW-FED multi-band omni-directional planar microstrip antenna using composite metamaterial resonators for wireless communications," *Progress In Electromagnetics Research*, PIER 83, 33–146, 2008.
6. Cho, K., T. Hori, H. Tozawa, and S. Kiya, "Bidirectional rod antennas comprising collinear antenna and parasitic elements," *IEICE Transactions on Communications*, No. 6, 1255–1260, 1998.
7. Cho, K., T. Hori, and K. Kagoshima, "Bidirectional rod antennas comprising a narrow patch and parasitic elements," *IEICE Transactions on Communications*, No. 9, 2482–2489, 2001.
8. Arai, H. and K. Cho, "Cellular and PHS base station antenna systems," *IEICE Transactions on Communications*, No. 9, 980–992, 2003.
9. Lamutree, S., C. Phongcharoenpanich, S. Kosulvit, and M. Krairiksh, "An equivalent circuit of a bidirectional antenna using a probe excited rectangular ring," *The Proceedings of the 2004 IEEE International Symposium on Antennas and Propagation and USNC/URSI National Radio Science Meeting*, Vol. 2, 1672–1675, 2004.
10. Lamutree, S., C. Phongcharoenpanich, S. Kosulvit, and M. Krairiksh, "Investigations of a bidirectional antenna using a probe excited rectangular ring," *The Proceedings of Asia-Pacific Microwave Conference 2005*, Vol. 5, 2943–2946, 2005.
11. Liu, H., B.-Z. Wang, and W. Shao, "Dual-band bi-directional pattern reconfigurable fractal patch antenna for millimeter wave

- application,” *International Journal of Infrared and Millimeter Waves*, Vol. 28, No. 1, 25–31, 2007.
12. Kosulvit, S., M. Krairiksh, C. Phongcharoenpanich, and T. Wakabayashi, “A simple and cost-effective bidirectional antenna using a probe excited circular ring,” *IEICE Transactions on Electronics*, Vol. E84-C, No. 4, 443–450, 2001.
 13. Phongcharoenpanich, C., T. Sroysuan, P. Wouchoum, S. Kosulvit, and M. Krairiksh, “An array of a probe excited circular ring radiating bidirectional pattern,” *The Proceedings of the 2002 IEEE International Symposium on Antennas and Propagation and USNC/URSI National Radio Science Meeting*, Vol. 2, 292–294, 2002.
 14. Kosulvit, S., M. Krairiksh, C. Phongcharoenpanich, and T. Wakabayashi, “A bidirectional antenna using a probe excited circular ring,” *The Proceedings of the 2001 Progress in Electromagnetics Research Symposium*, 423, 2001.
 15. Risser, J. R., *Microwave Antenna Theory and Design*, Mc-Graw-Hill, 1949.
 16. Yaghjian, A., “Approximate formulas for the far field and gain of open-ended rectangular waveguide,” *IEEE Transactions on Antennas and Propagations*, Vol. 32, No. 4, 378–384, 1984.
 17. Jia, H., K. Yoshitomi, and K. Yasumoto, “Rigorous analysis of rectangular waveguide junctions by fourier transform technique,” *Progress In Electromagnetics Research*, PIER 20, 263–282, 1998.
 18. Jia, H., K. Yoshitomi, and K. Yasumoto, “Rigorous analysis of E-/H-plane junctions in rectangular waveguides using fourier transform technique,” *Progress In Electromagnetics Research*, PIER 21, 273–292, 1999.
 19. El Sabbagh, M. and K. Zaki, “Modeling of rectangular waveguide junctions containing cylindrical posts,” *Progress In Electromagnetics Research*, PIER 33, 299–331, 2001.
 20. Li, L.-W., T.-X. Zhao, M.-S. Leong, and T.-S. Yeo, “A spatial-domain method of moments analysis of a cylindrical-rectangular chirostrip,” *Progress In Electromagnetics Research*, PIER 35, 165–182, 2002.
 21. Booty, M. R. and G. A. Kriegsmann, “Reflection and transmission from a thin inhomogeneous cylinder in a rectangular TE_{10} waveguide,” *Progress In Electromagnetics Research*, PIER 47, 263–296, 2004.
 22. Liang, J.-F., H.-C. Chang, and K. A. Zaki, “Coaxial probe modeling in waveguides and cavities,” *IEEE Transactions on*

- Microwave Theory and Techniques*, Vol. 40, No. 12, 2172–2180, 1992.
23. Yao, H.-W. and K. A. Zaki, “Modeling of generalized coaxial probes in rectangular waveguides,” *IEEE Transactions on Microwave Theory and Techniques*, Vol. 43, No. 12, 2805–2811, 1995.
 24. Tai, C. T., *Dyadic Green’s Functions in Electromagnetic Theory*, 2nd ed., IEEE Press, 1994.
 25. Tai, C. T. “On the eigenfunction expansion of dyadic Green’s function,” *The Proceedings of IEEE*, Vol. 61, 480–481, 1973.
 26. Moroney, D. T. and P. J. Cullen, “The Green’s function perturbation method for solution of electromagnetic scattering problems,” *Progress In Electromagnetics Research*, PIER 15, 221–252, 1997.
 27. Li, L.-W., M.-S. Leong, P.-S. Kooi, T.-S. Yeo, and K. H. Tan, “An analytic representation of dyadic Green’s functions for a rectangular chirowaveguide: Part I — Theory,” *IEEE Transactions on Microwave Theory and Techniques*, Vol. 47, No. 1, 67–73, 1999.
 28. Leong, M., K. H. Tan, L.-W. Li, P.-S. Kooi, and T.-S. Yeo, “An analytic representation of dyadic Green’s functions for a rectangular chirowaveguide: Part II — Results,” *IEEE Transactions on Microwave Theory and Techniques*, Vol. 47, No. 1, 74–81, 1999.
 29. Liu, S., L. W. Li, M. S. Leong, and T. S. Yeo, “Rectangular conducting waveguide filled with uniaxial anisotropic media: A modal analysis and dyadic Green’s function,” *Progress In Electromagnetics Research*, PIER 25, 111–129, 2000.
 30. Marliani, F. and A. Ciccolella, “Computationally efficient expressions of the dyadic Green’s function for rectangular enclosures,” *Progress In Electromagnetics Research*, PIER 31, 195–223, 2001.
 31. Balanis, C. A., *Antenna Theory Analysis and Design*, John Wiley & Sons, 1997.
 32. Balanis, C. A., *Advanced Engineering Electromagnetics*, John Wiley & Sons, 1989.
 33. Rao, S. M., D. R. Wilton, and A. W. Glisson, “Electromagnetic scattering by surfaces of arbitrary shape,” *IEEE Transactions on Antennas and Propagation*, Vol. AP-30, 409–418, 1982.